IEEE Photonics Journal
An IEEE Photonics Society Publication

Efficient Fiber-to-Waveguide Edge Coupling Using an Optical Fiber Axicon Lens Fabricated by Focused Ion Beam

Volume 9, Number 4, August 2017

Henrik Melkonyan
Karen Sloyan
Krishna Twayana
Paulo Moreira
Marcus S. Dahlem

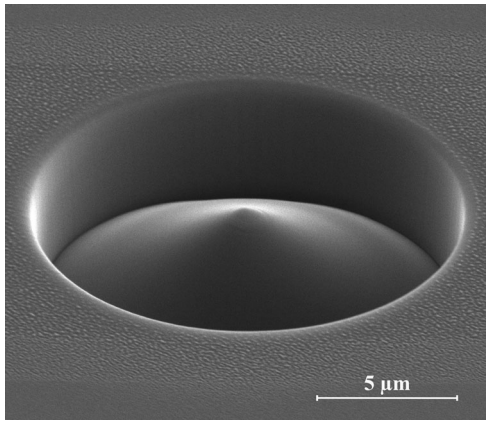

DOI: 10.1109/JPHOT.2017.2710189
1943-0655 © 2017 IEEE

Efficient Fiber-to-Waveguide Edge Coupling Using an Optical Fiber Axicon Lens Fabricated by Focused Ion Beam

Henrik Melkonyan, Karen Sloyan, Krishna Twayana, Paulo Moreira, and Marcus S. Dahlem

Nano-Optics and Optoelectronics Research Laboratory, Masdar Institute, Khalifa University of Science and Technology, Abu Dhabi, UAE

DOI:10.1109/JPHOT.2017.2710189

Manuscript received April 19, 2017; revised May 16, 2017; accepted May 26, 2017. Date of publication June 2, 2017; date of current version June 20, 2017. Corresponding author: Marcus S. Dahlem (e-mail: mdahlem@masdar.ac.ae).

Abstract: Efficient edge coupling into a silicon waveguide is demonstrated using an optical fiber axicon lens operating at 1550 nm. The axicon was fabricated on the cleaved endfacet of an SMF-28e optical fiber using a focused ion beam milling process. The lens converts the guided mode of the optical fiber (mode field diameter of 10.4 μm) into a Bessel-type beam with an extended depth of focus, which was verified both experimentally and by three-dimensional finite-difference time-domain simulations. Axicon lenses with a diameter of 15 μm and heights of 3.5 and 5.0 μm were fabricated, and their focusing effect optically characterized through high-resolution confocal imaging, showing a focal spot size of 3.57 and 2.34 μm, respectively. The coupling efficiency from the axicon into a silicon-on-insulator photonic integrated circuit is comparable to that of a commercial tapered lensed fiber, and in some cases slightly higher. Due to the extended depth of focus, the axicon lens also offers a larger alignment tolerance in the longitudinal direction.

Index Terms: Axicon lens, fiber optics, focused ion beam milling.

1. Introduction

Axicon lenses are known for efficiently generating Bessel-type beams [1], [2], and they can be used to convert a Gaussian beam into a zeroth-order Bessel beam with little diffraction, i.e., large depth of focus [3]. High-order Bessel beam generation has also been demonstrated with an axicon illuminated by a Laguerre-Gaussian beam [4]. Axicons can be classified as refractive [4]–[10] or diffractive [11]–[13]. Diffractive axicons are less efficient in transmitting light and the performance is strongly dependent on the wavelength [12], which make refractive axicons more popular. Axicons have been successfully applied in optical tweezers [5], [14], [15], material processing [10], [16] and non-linear optics [13]. In [7], [8], fiber microaxicons fabricated on the tip of an optical fiber were used to create a focused beam with a spot size near the diffraction limit. Several fabrication techniques have been demonstrated for fiber microaxicons, such as chemical etching [7]–[9], mechanical polishing [6], and micromachining using focused ion beam (FIB) milling [5]. While the chemical etching and polishing fabrication techniques remove most of the fiber tip material, creating a relief conical structure on the tip surface, the FIB milling process enables the fabrication of a microaxicon embedded below the tip surface of the fiber, with a more precise control of its geometry. In [5], the first fiber microaxicon fabricated using FIB was applied in optical trapping. The extended depth of

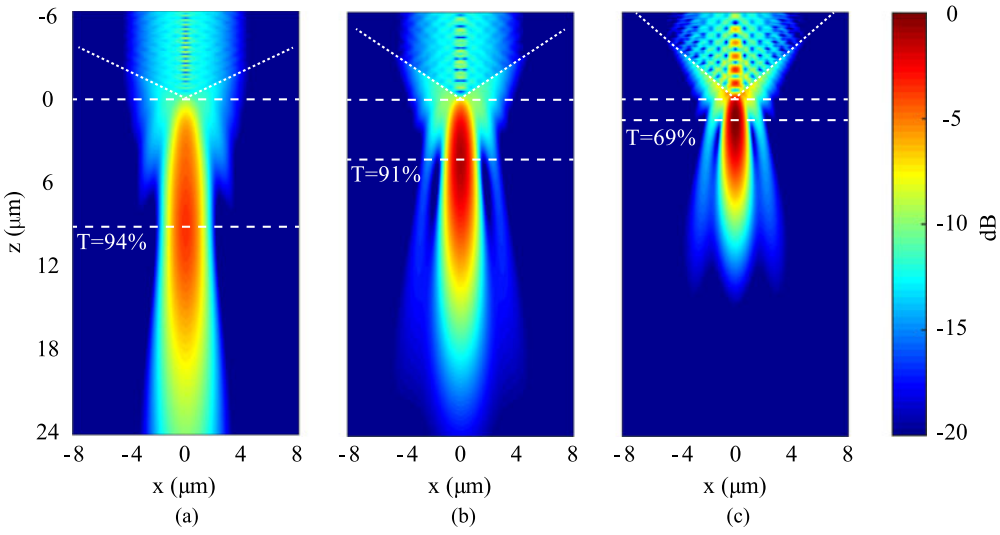

Fig. 1. Normalized intensity distribution (relative to the peak intensity) in the *xz* plane, determined by 3D FDTD simulations, for axicon fiber lenses with diameter $D = 15\ \mu$m and heights of (a) 3.5 μm ($\alpha = 130°$), (b) 5 μm ($\alpha = 113°$), and (c) 6.5 μm ($\alpha = 98°$). The top and bottom horizontal dashed lines indicate the location of the tip of the axicon and the working distance, respectively.

focus and small spot sizes generated by axicons also make them suitable for fiber-to-waveguide edge coupling applications, mainly when the mismatch between the input optical fiber mode and the waveguide mode is large. The coupling loss due to this mode mismatch is usually reduced using a tapered optical fiber lens that focuses the large fiber mode into a smaller spot. Other fiber lens solutions have been proposed and demonstrated, such as optical fiber lenses using diffractive elements [17]–[19], as well as concave fiber tips for mode conversion [20].

In this work, we use a fiber microaxicon lens fabricated by FIB milling to demonstrate efficient direct edge coupling into a silicon photonic integrated circuit (PIC). The axicon properties were studied by numerical simulations using the three-dimensional (3D) finite-difference time-domain (FDTD) method, and the optimal parameters for maximizing the coupling conditions were extracted. Optical characterization results of the fabricated fiber axicons are presented, as well as the coupling performance, which was compared with that of a standard commercial lensed fiber.

2. Design and Simulation

The design of the axicon was based on the optical properties of the single-mode optical fiber SMF-28e (Corning). The diameter and refractive index of the fiber core are 8.2 μm and $n_c = 1.4678$, respectively. The refractive index of the cladding is $n_{cl} = 1.4625$. The mode field diameter at a wavelength of 1550 nm is 10.4 μm. The diameter (D) of the fiber axicon was fixed at 15 μm, which is sufficiently large to cover the fiber mode area in order to achieve an efficient mode conversion. A larger axicon diameter would increase the fabrication time with only residual improvement in the conversion efficiency. The optical fiber axicon (with $D = 15\ \mu$m) was numerically simulated using the 3D FDTD method, for axicon heights between 3.5 μm and 7 μm, corresponding to axicon apex angles (α) between 130° and 94°, respectively. For axicons with larger heights (lower apex angles), we found that the focal spot would be located inside the axicon. At the fiber-air interface forming the axicon, the guided light undergoes total internal reflection, which creates a region of higher intensity inside the lens. In all our simulations, the fiber fundamental mode (at a wavelength of 1550 nm) was launched inside the fiber section of the designed structure, propagating along the longitudinal *z* axis.

Fig. 1 shows the intensity distribution along the direction of propagation, in the *xz* plane, for three axicons with heights 3.5 μm ($\alpha = 130°$), 5 μm ($\alpha = 113°$) and 6.5 μm ($\alpha = 98°$). The intensity

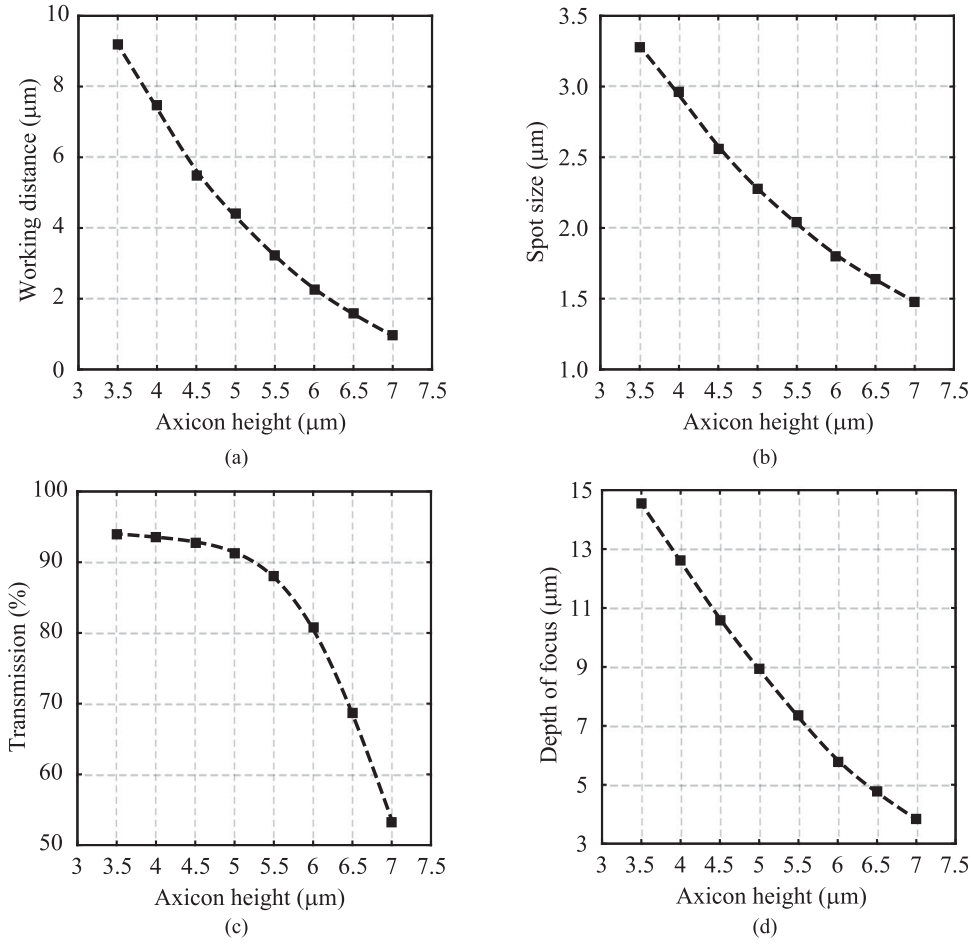

Fig. 2. Axicon optical properties, calculated numerically using the 3D FDTD method, as a function of the axicon height: (a) working distance, (b) spot size, (c) power transmission, and (d) depth of focus.

distribution of each axicon is normalized to the maximum intensity of the 6.5 μm-high axicon. The focusing effect, with a depth of focus inversely proportional to the axicon height, can be observed in the figure.

The axicon optical properties are assessed by determining the working distance, the spot size, the depth of focus, and the power transmission. Here, the working distance is defined as the distance between the axicon top edge (indicated in the figure by the horizontal dashed line at $z = 0$) and the location of the intensity maximum along the z axis (indicated by the bottom horizontal dashed line). The spot size can be evaluated from the intensity profile along the x axis at the working distance of the axicon, and is defined as the distance between the positions where the intensity drops to $1/e^2$ of its peak value. The depth of focus was determined as the distance along the propagation axis (z) between the positions where the spot size increases by a factor of $\sqrt{2}$ of its minimum value. The transmitted power was monitored in the xy plane at the working distance of the axicon lens. Fig. 2 summarizes the optical properties of the axicon lenses. Fig. 2(a) and (b) show how the working distance and the spot size of the axicon vary as a function of the axicon height. Within the studied range of axicon heights, the working distance varies from 9.18 μm to 0.96 μm, and the spot size decreases from 3.28 μm to 1.48 μm. Although the focal spot is smaller for the higher axicons, the power transmission is also lower due to higher reflections occurring at the axicon top fiber-air interface. This trend can be observed in Fig. 2(c): for axicon heights between 3.5 μm and 5 μm, the power transmission does not vary significantly (between 94% and 91%), but decays for axicons with

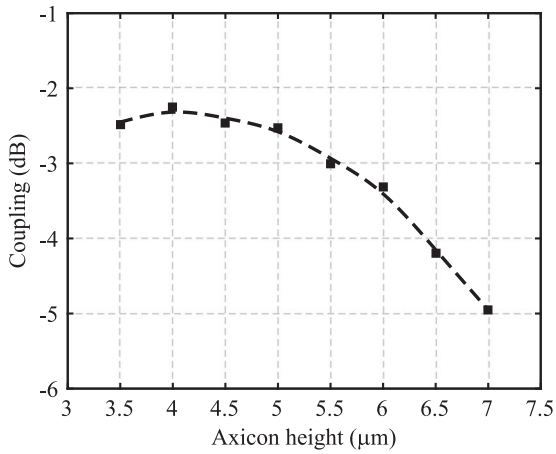

Fig. 3. Fiber-to-waveguide coupling efficiency calculated as a function of the axicon height, for TE polarization. The coupling is calculated between the axicon lens and a 200 nm $\times$ 220 nm silicon waveguide.

larger heights. Fig. 2(d) shows that axicons with smaller heights have an extended depth of focus. This property can be explored in direct fiber-to-waveguide edge coupling applications in order to increase the alignment tolerance in the longitudinal direction, relative to that found with tapered lensed fibers.

Here, we focus on TE-polarized light coupling from the axicon lens into a silicon waveguide with a cross-section of 200 nm $\times$ 220 nm (which is the edge of an inverted taper spot size converter designed to optimize TE-polarized light coupling with a lensed fiber). Fig. 3 shows the computed coupling efficiency between the spot generated by the axicon and the TE mode of the silicon waveguide, as a function of the axicon height. The coupling is higher for axicons with heights between 3.5 μm and 5 μm. As pointed out, although axicons with larger heights generate smaller spots, the power transmission is also significantly lower, which explains the decrease in the overall coupling efficiency.

3. Fabrication

The axicon fiber lenses were fabricated by focused ion beam milling using an FEI Quanta 3D FEG/FIB Dual Beam system. The protective polymer layer of a standard single-mode fiber (Corning SMF-28e) was first removed, and the fiber vertically mounted on a metallic sample holder. In order to avoid ion beam induced charging of the sample during the milling procedure, a 30 nm-thick gold/palladium film was sputtered onto the surface of the fiber/holder system. The metallic film dissipates the excess charges from the fiber to the metallic sample holder. The axicon structure was designed as a gray-scale pattern, where gray-scale levels were associated with different dwell times for the ion beam exposure. The milling procedure was carried out over a 15 μm-diameter region centered at the fiber core, using 30 keV accelerated Ga^+ ions. A probe current of 0.5 nA was used during the entire milling process. After optimization, the maximum dwell time and volume per dose were determined to be 5 μs and 0.52 μm^3/nC, respectively. Axicon lenses with different heights can be fabricated through different ion beam exposure times. In this work, two axicon fiber lenses, with heights of 3.5 μm and 5 μm, were fabricated. Fig. 4 shows scanning electron microscopy (SEM) images of the 5 μm-high axicon fabricated on the cleaved endfacet of the optical fiber.

4. Optical Characterization and Waveguide Coupling

The fabricated lenses were characterized through high-resolution confocal imaging, at a wavelength of 1550 nm, using a high numerical aperture tapered lensed fiber (from Nanonics) as a scanning

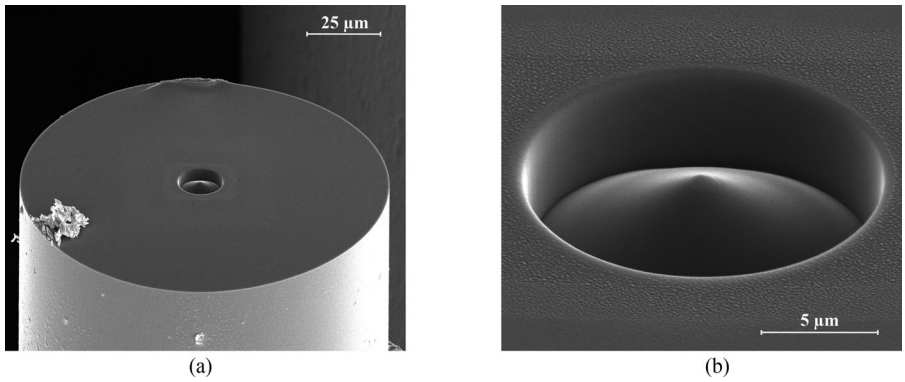

Fig. 4. SEM images of a 5 μm-high axicon lens fabricated on the tip of a single-mode optical fiber: (a) axicon lens located at the center of the fiber endfacet, and (b) magnified view of the axicon lens.

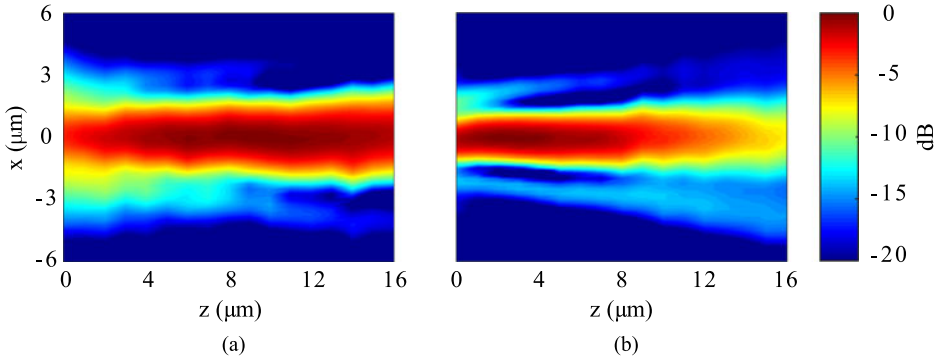

Fig. 5. Spatial intensity distribution of the focused beam in the *xz* plane at 1550 nm, for axicons with a diameter of 15 μm and heights of (a) 3.5 μm and (b) 5 μm.

probe, with a measured spot size of 1,85 μm and a working distance around 4 μm. Both the axicon lens and the tapered lensed fiber were mounted on high-precision, piezo-controlled, three-axis micropositioning stages. The beam evolution, after exiting the fiber axicon, was analyzed by acquiring subsequent cross-sectional intensity distribution images at positions distanced by 1 μm along the direction of propagation (*z* axis). At each position, the intensity distribution image was recorded from an *xy* scan with a lateral step size of 0.25 μm. Fig. 5 shows the reconstructed spatial intensity distribution in the *xz* plane for the two fabricated axicons. As expected, the spot size, working distance and depth of focus are inversely proportional to the axicon height. However, the working distance of the axicons could not be accurately evaluated since the scanning procedure started at an unknown safe distance between the fiber axicon and the scanning probe, identified as $z = 0$ in the figure.

The measured and simulated field intensity cross-sections at the working distance, for the two fabricated axicons, are shown in Fig. 6. A zeroth-order Bessel-type profile is confirmed, showing an intense central lobe and less intense outward concentric rings. The slight distortion, observed in the spot cross-section of the fabricated axicons, is either due to a small angular misalignment between the axicon axis and the probe, or due to an axicon asymmetry resulting from fabrication. Fig. 6(c) and (f) compare the normalized intensity profiles along the *x* axis of the measured and simulated focal spots for both axicon lenses. The measured profiles are slightly wider, which can be the result of the convolution between the true axicon profiles and the probe response. To estimate the experimental spot size (as the width at $1/e^2$ from the peak intensity), the measured profiles were deconvolved from the response of the lensed fiber. The axicons with heights of 3.5 μm and 5 μm

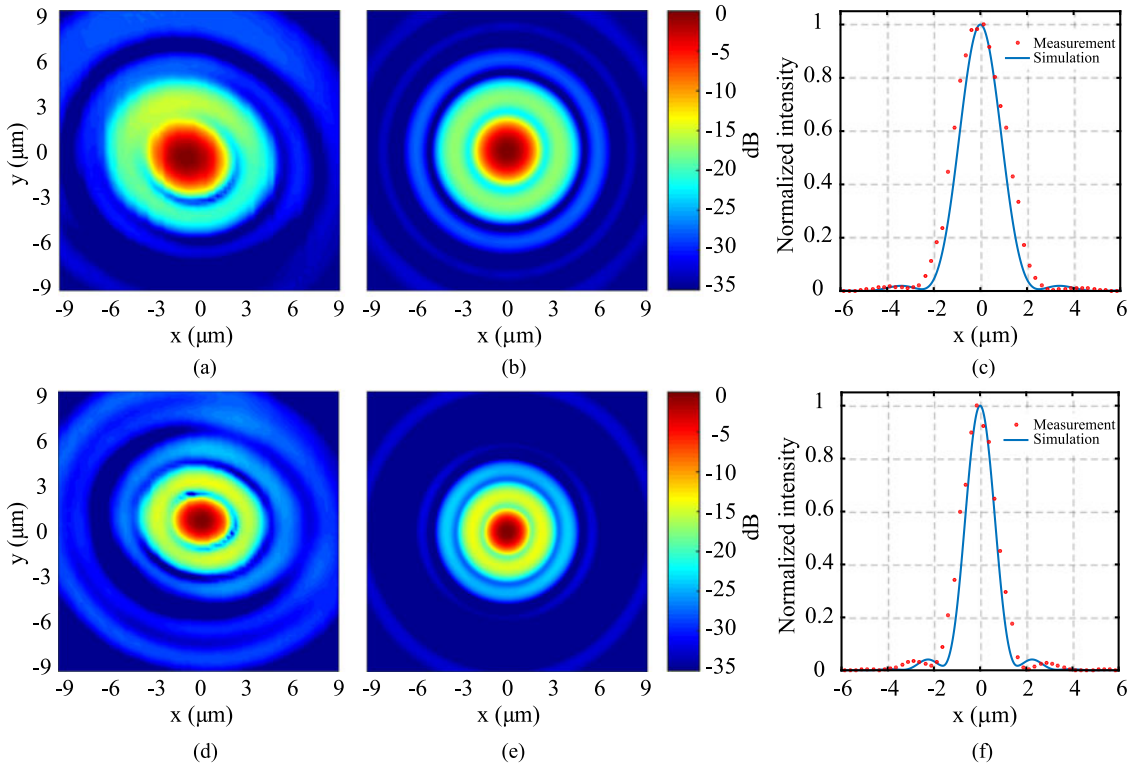

Fig. 6. Focusing performance of the axicons at 1550 nm: (a) measured confocal image, and (b) FDTD computed intensity distribution of the beam cross-section at the focal plane for the 3.5 μm-high axicon lens; (c) measured and simulated line profiles along the *x* axis for the 3.5 μm-high axicon lens, with a measured spot size of 3.57 μm; (d) measured confocal image, and (e) FDTD computed intensity distribution of the beam cross-section at the focal plane for the 5 μm-high axicon lens; (f) measured and simulated line profiles along the *x* axis for the 5 μm-high axicon lens, with a measured spot size of 2.34 μm.

generated beam spots with diameters of 3.57 μm and 2.34 μm, respectively, which are consistent with the simulated values presented in Fig. 2(b).

The coupling performance of the fabricated axicons was experimentally evaluated using a polarization-controlled setup for characterizing silicon photonics chips. The light source is a linearly polarized tunable laser (1 mW power) emitting at a wavelength of 1550 nm. Both straight waveguides and ring resonator add-drop filters were used for the test. At both sides (input and output), the chip has inverted tapers as spot size converters. The waveguides at both edges have a cross-section of 200 nm $\times$ 220 nm and support a slightly leaky TE mode with a mode size around 1 μm. The over- and under-cladding consist of a 2 μm-thick silicon dioxide layer. The axicon fiber lens was used to couple light into the waveguide, and the output light was collected by a standard commercial tapered lensed fiber. The polarization was set with an electronic polarization controller. The coupling performance of both axicon fibers was measured in a straight waveguide as a function of the distance from the waveguide edge, and compared with the performance of the lensed fiber. The measurement was performed for TE polarization, and the results are presented in Fig. 7. In the figure, the origin ($z = 0$) corresponds to the longitudinal position where the coupling power is maximum (working distance). The transmission was measured for different separations between the fiber and the waveguide in steps of 1 μm, up to 15 μm. The 5 μm-high axicon slightly outperforms the lensed fiber within the entire studied range (15 μm). The figure also shows that the longitudinal alignment tolerance is better for the axicons. The coupled power decreases by 0.1 dB/μm and 0.2 dB/μm, for the 5 μm-high and 3.5 μm-high axicons, respectively, while the value for the lensed

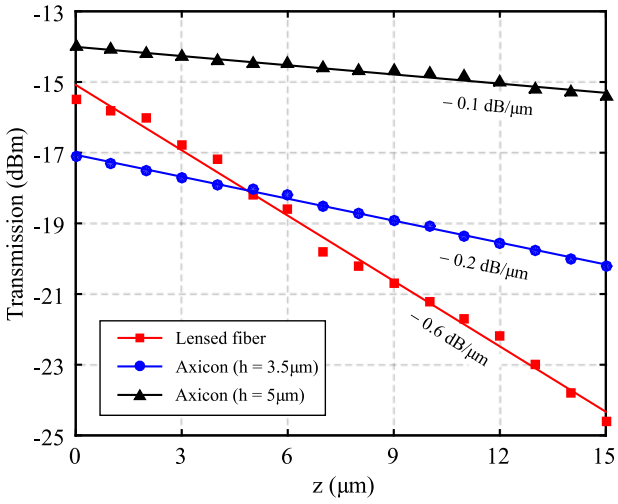

Fig. 7. Measured transmission in a straight waveguide for TE polarization at 1550 nm, coupled from the fabricated axicons (with heights of 3.5 μm and 5 μm) and from a tapered lensed fiber, as a function of the separation between each fiber tip and the silicon waveguide. $z = 0$ corresponds to the working distance.

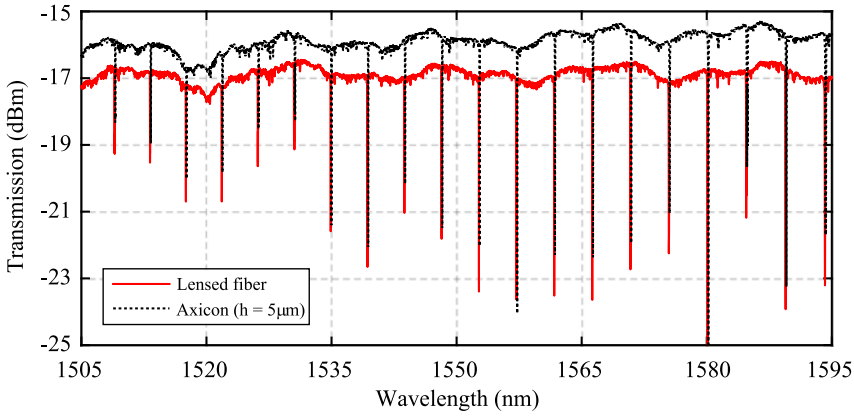

Fig. 8. Power transmission at the add-drop filter through port, for TE polarization, when the input coupling fiber is switched between the 5 μm-high axicon (dashed line) and the tapered lensed fiber (solid line).

fiber is approximately 0.6 dB/μm. Over 15 μm, this corresponds to a reduction in coupling of up to 3.1 dB for the axicons, compared to 9 dB for the lensed fiber, confirming the increased longitudinal alignment tolerance of the axicon lenses.

Comparing the two axicon lenses, the reduction of the coupling efficiency is larger for the 3.5 μm-high axicon (0.2 dB/μm), despite the larger depth of focus (see Fig. 5). Furthermore, the coupling efficiency at the working distance ($z = 0$) for the 3.5 μm-high axicon is lower than expected (according to Fig. 3). In fact, the measured focal spot size of the 3.5 μm-high axicon is 3.57 μm, which is slightly larger than the calculated one (3.28 μm). A reduction of the coupling efficiency for axicons with heights lower than 3.5 μm (larger focal spot) is expected. In the optimal coupling condition, the coupling sensitivity (derivative of the curve in Fig. 3) to spot size variations (due to longitudinal displacement) is not significant. However, a deviation from this optimal coupling condition (which is likely the case for the 3.5 μm-high axicon) would result in an increased sensitivity. When the coupling sensitivity is higher, a smaller variation of the spot size will therefore result in a larger reduction (in dB/μm) of the coupling efficiency. This deviation is not observed in the 5 μm-high axicon. Regarding the lateral (xy) alignment tolerance, it is similar for the 5 μm-high axicon and for

the tapered lensed fiber. However, due to the larger spot size, the 3.5 μm-high axicon lens offers a higher lateral tolerance.

The coupling performance was also confirmed in a ring resonator add-drop filter (ring and bus waveguides width $=$ 450 nm, ring radius $=$ 20 μm, and ring-bus gap $=$ 300 nm) in the wavelength range of 1505 nm to 1595 nm. Fig. 8 compares the transmission response of the filter through port for TE polarization, for the 5 μm-high axicon fiber and the tapered lensed fiber. In this measurement, the output tapered lensed fiber was maintained. We verified that the coupling is slightly improved with the 5 μm-high axicon over the entire wavelength range, in comparison to the tapered lensed fiber (between 0.5 dB at lower wavelengths up to 1.4 dB at larger wavelengths). Using the 5 μm-high axicon fiber at both input and output of the device, the insertion loss could be reduced up to 2.8 dB. Ideally, the tapered lensed fiber should provide a higher coupling performance due to the smaller focal spot (1.85 μm vs. 2.34 μm). However, the performance of the lensed fiber is highly sensitive to the nature of the fabrication process. The measured cross-sectional intensity distribution of the lensed fiber at the working distance revealed some scattering which was less pronounced in the axicon lenses.

5. Conclusion

In this work, we fabricated an axicon on the tip of an SMF-28e optical fiber for coupling light into a silicon PIC with efficiencies comparable to commercial lensed fibers. The axicon lens was fabricated by focused ion beam milling. The axicon produces a Bessel-type beam with an extended depth of focus, which results in a better alignment tolerance in the longitudinal direction (0.1 dB/μm for the 5 μm-high axicon vs. 0.6 dB/μm for the lensed fiber). The axicon performance was studied as a function of its height, and a good agreement between the experimental and simulated intensity distributions of the focused spots was obtained. The 5 μm-high axicon reduced the insertion loss of a silicon device by up to 1.4 dB, compared to a commercial lensed fiber. Although the coupling efficiency improvement is moderate, the major advantage of the axicon is the larger longitudinal alignment tolerance and its mechanical robustness.

References

[1] J. Durnin, J. Miceli Jr., and J. Eberly, "Diffraction-free beams," *Phys. Rev. Lett.*, vol. 58, no. 15, pp. 1499–1501, 1987.
[2] J. Durnin, "Exact solutions for nondiffracting beams. I. The scalar theory," *J. Opt. Soc. Amer. A*, vol. 4, no. 4, pp. 651–654, 1987.
[3] M. Duocastella and C. B. Arnold, "Bessel and annular beams for materials processing," *Laser Photon. Rev.*, vol. 6, no. 5, pp. 607–621, 2012.
[4] J. Arlt and K. Dholakia, "Generation of high-order Bessel beams by use of an axicon," *Opt. Commun.*, vol. 177, no. 1, pp. 297–301, 2000.
[5] S. Cabrini *et al.*, "Axicon lens on optical fiber forming optical tweezers, made by focused ion beam milling," *Microelectron. Eng.*, vol. 83, no. 4, pp. 804–807, 2006.
[6] T. Grosjean *et al.*, "Fiber microaxicons fabricated by a polishing technique for the generation of Bessel-like beams," *Appl. Opt.*, vol. 46, no. 33, pp. 8061–8067, 2007.
[7] S.-K. Eah, W. Jhe, and Y. Arakawa, "Nearly diffraction-limited focusing of a fiber axicon microlens," *Rev. Sci. Instrum.*, vol. 74, no. 11, pp. 4969–4971, 2003.
[8] A. Kuchmizhak, S. Gurbatov, A. Nepomniaschii, O. Vitrik, and Y. Kulchin, "High-quality fiber microaxicons fabricated by a modified chemical etching method for laser focusing and generation of Bessel-like beams," *Appl. Opt.*, vol. 53, no. 5, pp. 937–943, 2014.
[9] K. Bachus, E. S. de Lima Filho, K. Wlodarczyk, R. Oleschuk, Y. Messaddeq, and H.-P. Loock, "Fabrication of axicon microlenses on capillaries and microstructured fibers by wet etching," *Opt. Exp.*, vol. 24, no. 18, pp. 20 346–20 358, 2016.
[10] A. Marcinkevičius, S. Juodkazis, S. Matsuo, V. Mizeikis, and H. Misawa, "Application of Bessel beams for microfabrication of dielectrics by femtosecond laser," *Jpn. J. Appl. Phys.*, vol. 40, no. 11A, pp. L1197–L1199, 2001.
[11] I. Golub, "Fresnel axicon," *Opt. Lett.*, vol. 31, no. 12, pp. 1890–1892, Jun. 2006.
[12] E. Bialic and J.-L. de Bougrenet de la Tocnaye, "Multiple annular linear diffractive axicons," *J. Opt. Soc. Amer. A*, vol. 28, no. 4, pp. 523–533, 2011.
[13] T. Wulle and S. Herminghaus, "Nonlinear optics of Bessel beams," *Phys. Rev. Lett.*, vol. 70, no. 10, pp. 1401–1404, 1993.
[14] S. Mohanty, K. Mohanty, and M. Berns, "Organization of microscale objects using a microfabricated optical fiber," *Opt. Lett.*, vol. 33, no. 18, pp. 2155–2157, 2008.

[15] X. Tsampoula *et al.*, "Fibre based cellular transfection," *Opt. Exp.*, vol. 16, no. 21, pp. 17007–17013, 2008.
[16] D. McGloin and K. Dholakia, "Bessel beams: Diffraction in a new light," *Contemp. Phys.*, vol. 46, no. 1, pp. 15–28, 2005.
[17] F. Schiappelli *et al.*, "Efficient fiber-to-waveguide coupling by a lens on the end of the optical fiber fabricated by focused ion beam milling," *Microelectron. Eng.*, vol. 73, pp. 397–404, 2004.
[18] M. Prasciolu *et al.*, "Design and fabrication of on-fiber diffractive elements for fiber-waveguide coupling by means of e-beam lithography," *Microelectron. Eng.*, vol. 67–68, pp. 169–174, 2003.
[19] R. Janeiro, R. Flores, P. Dahal, and J. Viegas, "Fabrication of a phase photon sieve on an optical fiber tip by focused ion beam nanomachining for improved fiber to silicon photonics waveguide light coupling," *Opt. Exp.*, vol. 24, no. 11, pp. 11611–11625, 2016.
[20] M. Mayeh and F. Farahi, "Laser beam shaping and mode conversion in optical fibers," *Photon. Sensors*, vol. 1, no. 2, pp. 187–198, 2011.